HHS Public Access

Author manuscript

Cell Metab. Author manuscript; available in PMC 2016 April 07.

Published in final edited form as:

Cell Metab. 2015 April 7; 21(4): 609–621. doi:10.1016/j.cmet.2015.03.006.

IGF2BP2/IMP2 Deficient Mice Resist Obesity through enhanced translation of *Ucp1* mRNA and other mRNAs encoding Mitochondrial Proteins

Ning Dai[1,2,4], **Liping Zhao**[1,2,4], **Diedra Wrighting**[1,5,8], **Dana Krämer**[9], **Amit Majithia**[1,2,4,8], **Yanqun Wang**[1], **Valentin Cracan**[1,6], **Diego Borges-Rivera**[1,5,8], **Vamsi K. Mootha**[1,2,4,6], **Matthias Nahrendorf**[3,7], **David R. Thorburn**[11,12], **Liliana Minichiello**[9,10,‡], **David Altshuler**[1,2,4,5,8,‡,*], and **Joseph Avruch**[1,2,4,‡,*]

[1]Department of Molecular Biology, Massachusetts General Hospital, Boston, Massachusetts 02114, USA

[2]Diabetes Unit, Medical Services, Massachusetts General Hospital, Boston, Massachusetts 02114, USA

[3]Department of Radiology and the Center for Systems Biology, Massachusetts General Hospital, Boston, Massachusetts 02114, USA

[4]Department of Medicine, Harvard Medical School, Boston, Massachusetts 02115, USA

[5]Department of Genetics, Harvard Medical School, Boston, Massachusetts 02115, USA

[6]Department of Systems Biology, Harvard Medical School, Boston, Massachusetts 02115, USA

[7]Department of Radiology, Harvard Medical School, Boston, Massachusetts 02115, USA

[8]Program in Medical and Population Genetics, Broad Institute of Harvard and MIT, Cambridge, Massachusetts 02142, USA

[9]European Molecular Biology Laboratory, Mouse Biology Unit, 00015-Monterotondo, Italy

[10]Department of Pharmacology, University of Oxford, OX1 3QT, Oxford, UK

[11]Murdoch Childrens Research Institute and Victorian Clinical Genetics Services, Royal Children's Hospital, Flemington Road, Parkville, Melbourne, VIC 3052, Australia

[12]Department of Paediatrics, University of Melbourne, Melbourne, VIC 3010, Australia

Abstract

[*]To whom correspondence should be addressed: Joseph Avruch M.D., Department of Molecular Biology, Massachusetts General Hospital, Department of Medicine, Harvard Medical School, Simches Research Bldg 6408, 185 Cambridge St., Boston, MA 02114, Tel:617-726-6909, Fax:617-726-5649, avruch@molbio.mgh.harvard.edu, David Altshuler MD, PhD, Department of Molecular Biology, Massachusetts General Hospital, Department of Genetics, Harvard Medical School Hospital, Medical and Population Genetics Broad Institute of Harvard and MIT, Simches Research Building CPZN 6818, 185 Cambridge St., Boston, MA 02114, Tel: 617 726-5940, Fax: 617-643-3293, altshuler@molbio.mgh.harvard.edu.

[‡]Equal contributions

Although variants in the *IGF2BP2/IMP2* gene confer risk for Type 2 diabetes, IMP2, an RNA binding protein, is not known to regulate metabolism. *Imp2*$^{-/-}$ mice gain less lean mass after weaning and have increased lifespan. *Imp2*$^{-/-}$ mice are highly resistant to diet-induced obesity and fatty liver and display superior glucose tolerance and insulin sensitivity, increased energy expenditure and better defense of core temperature on cold exposure. *Imp2*$^{-/-}$ brown fat and *Imp2*$^{-/-}$ brown adipocytes differentiated in vitro contain more UCP1 polypeptide than *Imp2*$^{+/+}$ despite similar levels of *Ucp1* mRNA; the *Imp2*$^{-/-}$ adipocytes also exhibit greater uncoupled oxygen consumption. IMP2 binds the mRNAs encoding *Ucp1* and other mitochondrial components, and most exhibit increased translational efficiency in the absence of IMP2. In vitro IMP2 inhibits translation of mRNAs bearing the *Ucp1* untranslated segments. Thus IMP2 limits longevity and regulates nutrient and energy metabolism in the mouse by controlling the translation of its client mRNAs.

Graphical Abstract

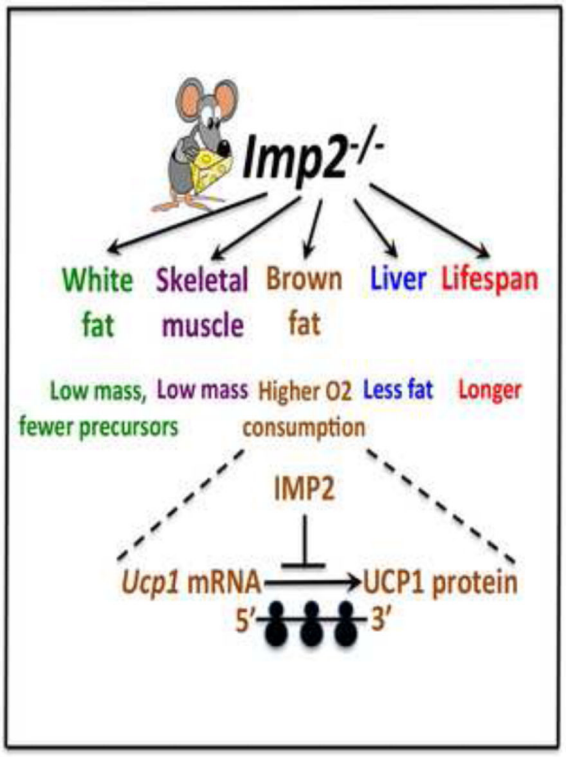

Introduction

Susceptibility to Type 2 diabetes mellitus (T2DM) is strongly influenced by both environmental (Knowler et.al., 2002) and genetic factors (DIAGRAM Consortium, 2014). Genome-wide association studies (GWAS) have mapped over seventy genomic locations at which common single nucleotide polymorphisms (SNPs) are associated with risk of T2D. Most variants map to noncoding regions making it difficult to implicate specific gene(s) and mechanisms at each locus. One of the first SNPs found by GWAS for T2DM is located in

intron 2 of the gene encoding the RNA binding protein, IGF2 mRNA binding protein 2, abbreviated IGF2BP2 or IMP2 (Saxena et.al., 2007; Zeggini et.al., 2007; Scott et.al., 2007).

IMP1-3, named for their ability to bind to the leader 3 5'UTR of human *IGF2* mRNA (Nielsen et.al., 1999), participate in post-transcriptional RNA processing i.e., RNA splicing, stabilization, transport and translation (Yisraeli, 2005) Considered "oncofetal" proteins, expression of *Imp1-3* in the mouse embryo peaks coordinately at ~e12.5 (Nielsen et.al., 1999), coinciding with the expression of IGF2 polypeptide. Whereas the expression of *Imp1* and *3* is largely extinguished before birth (Nielsen et.al., 1999), *Imp2* expression is widespread in the adult mouse (Dai et.al., 2011). Imp2 is phosphorylated by mTOR complex1 in a rapamycin-sensitive manner (Dai et.al., 2011) and transgenic overexpression of IMP2 in mouse liver results in steatosis (Tybl et.al., 2011). Nevertheless, little is known of IMP2's physiologic functions and it is unclear whether and how the function of IMP2 relates to the association with T2D of an intronic SNP in the *IMP2* gene.

To determine whether IMP2 contributes to metabolism, we generated and characterized mice whose *Imp2* gene is inactivated. *Imp2*$^{-/-}$ mice resist diet-induced obesity and fatty liver due in part to increased energy expenditure and have a prolonged lifespan. *Imp2*$^{-/-}$ mice exhibit superior defense of body temperature when placed at 4°C, accompanied by an increased abundance of. IMP2 binds the *Ucp1* mRNA and whereas The abundance of uncoupling protein-1 (UCP1) in *Imp2*$^{-/-}$ brown fat is increased whereas *Ucp1* mRNA is not altered. IMP2 binds *Ucp1* mRNA and inhibits *Ucp1 mRNA* translation. The loss of IMP2 and the consequent increase in energy expenditure due to increased UCP1 contributes to a resistance to obesity, a beneficial metabolic profile and an increased lifespan.

Results

IMP2 abundance is regulated by nutrition

IMP2 is widely expressed in the adult mouse (Dai et.al., 2011). While an overnight fast decreases IMP2 abundance in liver (Fig. 1A), a high fat diet increases the abundance of IMP2 in liver and white adipose tissue (WAT, Fig.1B, upper), and IMP2 abundance is higher in the fat pads of *Lep*$^{-/-}$ mice (Fig. 1B, lower). Thus, increased intake and/or deposition of fat is accompanied by a leptin-independent increase in IMP2 abundance.

Imp2$^{-/-}$ mice are lean and resistant to diet-induced obesity

Imp2$^{-/-}$ mice (Fig. 1C, Fig.S1) are born at the expected Mendelian ratio, appear normal at birth, survive without difficulty, and are similar in weight to wildtype at weaning (4 weeks age). On normal chow diet (NCD) *Imp2* $^{-/-}$ mice gain less weight thereafter: at 30 weeks age, the *Imp2*$^{-/-}$ mice weigh approximately 25% less than wildtype littermates (Fig. 1D). Moreover, on a high fat diet (HFD) the difference in weight gain between male *Imp2*$^{-/-}$ and wildtype littermates is exaggerated (Fig. 1D, lower left). Analysis of body composition by magnetic resonance imaging (ECHO-MRI) shows that whereas wildtype mice gain approximately 17 gms in fat between weaning and 28 weeks age, the *Imp2*$^{-/-}$ males gain approximately 6 gms fat (Fig. 1E, upper). *Imp2*$^{-/-}$ females on a HFD are also lean (Fig. 1D, lower right). Thus the IMP2 deficient mice are relatively resistant to diet induced obesity.

Imp2$^{-/-}$ mice gain less lean mass after weaning and are longer-lived than wildtype

Imp2$^{-/-}$ mice gain lean mass at a slower rate of than wildtype, especially after 12 weeks age (Fig.1E, lower). The lean mass of *Imp2*$^{-/-}$ males is ~15% lower at 16 weeks and ~25% lower at 28 weeks, along with a 5% reduction in crown-rump length (males at 14 weeks on normal chow: wildtype 9.8+/−0.2 cm vs KO 9.3+/−0.16 cm, p=0.02). The smaller lean mass of the *Imp2*$^{-/-}$ mice reflects a proportionate reduction in size; direct measurement of organ weights from mice maintained on a high fat diet, when expressed as a fraction of body weight, shows that only the mass of the white adipose depots and the testes are selectively diminished; the weight of interscapular brown fat is similar (Fig. 1F). At all times, the fraction of body weight contributed by fat mass is lower in the *Imp2*$^{-/-}$ than in wildtype mice.

Genetic modifications in mice that are associated with a smaller, leaner phenotype (such as seen in the *Imp2*$^{-/-}$) have been associated with an extended lifespan. We maintained cohorts of wildtype and *Imp2*$^{-/-}$ mice on a normal chow without intervention: *Imp2*$^{-/-}$ mice exhibit a significantly longer median lifespan than wildtype littermates, both in males and females (Fig. 1G). As compared to wild-type littermates, the median survival of *Imp2*$^{-/-}$ males was 120 days longer (846 vs 726 days) and of *Imp2*$^{-/-}$ females 183 days longer (943 days vs 760 days). Maximum lifespan of *Imp2*$^{-/-}$ mice is also increased. The age at 90% survival was 885 and 986 days for male wildtype and *Imp2*$^{-/-}$ mice respectively, and 940 and 1023 days for female wildtype and *Imp2*$^{-/-}$ mice (including 2 *Imp2*$^{-/-}$ females alive at 1113 and 116 days). Combining the sexes, the last surviving 10% were comprised of 2/58 wildtype and 10/65 *Imp2*$^{-/-}$ mice, p=0.03 (Wang et.al., 2004). A caveat to the robust lifespan extension of the *Imp2*$^{-/-}$ mice as compared with wildtype is that the median lifespan of our wildtype C57Bl/6J cohort, although comparable to many earlier observations (mentioned in Turturro and Hart, 2002) is shorter than that in several recent reports (Turturro and Hart, 2002; http://research.jax.org/faculty/harrison/ger1vi_LifeStudy1.html).

Necropsy was performed on an apparently healthy cohort of six *Imp2*$^{+/+}$ and six *Imp2*$^{-/-}$ mice (5 males and one female of each genotype, all between 845–850 days age), taken from a cohort of several litters born in the same week and sacrificed at a time when ~20% of the *Imp2*$^{-/-}$ birth cohort had expired. Malignant tumors were detected in 4/6 *Imp2*$^{+/+}$ mice whereas no malignancies were detected in the six *Imp2*$^{-/-}$ mice. Histopatologic findings at necropsy for the individual mice are found in the experimental procedures.

Imp2$^{-/-}$ mice are resistant to fatty liver

We examined the histology of tissues important to the regulation of nutrient metabolism. Skeletal muscle of wildtype and *Imp2*$^{-/-}$ mice was indistinguishable by light or electron microscopic examination (not shown). Pancreatic morphology was normal in the *Imp2*$^{-/-}$ mice; immuno-histochemical stains for insulin and glucagon revealed a comparable abundance of normal appearing islets with a similar staining for glucagon in *Imp2*$^{-/-}$ and wildtype but a weaker signal for insulin in the *Imp2*$^{-/-}$ (Fig.2A), consistent with their lower serum insulin level (see below). H&E sections of formalin-fixed white adipose tissue show little or no difference in adipocyte size between *Imp2*$^{-/-}$ and wildtype mice, whether on normal chow or a high fat diet (Fig.2B), a finding confirmed by sizing of osmium tetroxide-

fixed adipocytes (Fig. S2A). The smaller white fat depots in HFD-fed *Imp2*$^{-/-}$ are thus due to fewer adult adipocytes, accompanied by a reduced number of Lin-CD29+CD34+ Sca1+ preadipocytes in the stromal-vascular compartment (Rodeheffer et.al.,2013); the ability of the *Imp2*$^{-/-}$ adipocyte precursors to proliferate and differentiate in vitro however is not different than wildtype (Fig. S2B-G). The morphology of interscapular brown adipose tissue is similar in wildtype and *Imp2*$^{-/-}$ mice fed normal chow (not shown), however after 8 weeks on a high fat diet the interscapular brown fat of wildtype mice has a distinctly more pale appearance than the *Imp2*$^{-/-}$ brown fat (Fig. 2C, left), due in part to greater fat deposition (Fig. 2C, right).

The most striking difference in histologic appearance between wildtype and *Imp2*$^{-/-}$ mice is found in the liver of mice fed the HFD. As expected, there was abundant deposition of fat in the liver of wildtype mice fed the HFD. In contrast, little fat is seen in the liver of *Imp2*$^{-/-}$ mice (Fig. 2D, left). This histological appearance was confirmed by direct measurement of liver triglyceride (Fig. 2D, right). The hepatic transcriptional response to the HFD was examined using high-throughput sequencing of RNA extracted from the livers of wildtype and *Imp2*$^{-/-}$ mice placed on normal chow or a HFD immediately after weaning and sacrificed one week later. Focusing on gene products relating to fatty acid and triglyceride metabolism (Fig. 2E), the modest differences evident on normal chow are largely eliminated by the HFD, suggesting that the lesser triglyceride deposition in the *Imp2*$^{-/-}$ liver is not attributable to an altered transcriptional response.

Imp2 null mice are hypolipidemic, glucose tolerant and insulin sensitive

In *Imp2*$^{-/-}$ mice, serum free fatty acids (FFA), triglyceride (TG) and total cholesterol (Table S1) were lower after a six hour (FFA/TG) or overnight (cholesterol) fast, on both normal chow or a HFD, and at all ages examined. On normal chow, blood glucose, whether taken at 7AM after feeding or after an overnight fast was significantly lower in the *Imp2*$^{-/-}$ after four weeks age (Fig. 3A). On a high fat diet, the *Imp2*$^{-/-}$ mice exhibited lower values of fasting glucose (Fig. 3A, Table S1) accompanied by lower levels of serum insulin (Table S1). Intraperitoneal glucose tolerance tests were performed on mice approximately 12–14 weeks age fed a HFD from weaning; *Imp2*$^{-/-}$ mice exhibited consistently lower values of glucose and insulin (Fig. 3B).

The presence of greater insulin sensitivity in the *Imp2*$^{-/-}$ was confirmed by the insulin tolerance test (Fig. 3C); at a dose of 0.4U/kg, the *Imp2*$^{-/-}$ mice showed a significantly greater decrease in blood glucose. The abundance of the insulin receptor beta subunit in liver, muscle and WAT does not differ between wildtype and *Imp2*$^{-/-}$ mice, whereas a supramaximal dose of insulin (5U/kg IP) induces greater relative phosphorylation of Akt(S473) and S6K1(T389) in the tissues of the *Imp2*$^{-/-}$ mice, (Fig.3D, E) providing further evidence of their greater insulin responsiveness.

A variety of other hormonal measurements at different ages on normal chow and on a HFD are shown in Table S2. Importantly, serum IGF1 and IGFBP3 levels, measured at 4 weeks in males (Table S2) and at 7–8 weeks age in females (not shown) are not different in wildtype and *Imp2*$^{-/-}$.

Imp2$^{-/-}$ mice have increased energy expenditure but normal food intake, fat absorption and physical activity

We next sought to define the basis for the greatly diminished fat deposition in the *Imp2*$^{-/-}$ mice, especially when maintained on the high fat diet (HFD). Food intake was measured on NCD and HFD, at several ages between 6–20 weeks, and over intervals lasting 2–3 days up to 4 weeks (Fig. 4A,B, Fig. S3A). No differences were observed in the food intake of the wildtype and *Imp2*$^{-/-}$ littermates. The percent of fecal weight as fat was determined on both diets in mice 17–20 weeks age (Fig. 4C), and was no different in the wildtype and *Imp2*$^{-/-}$ mice (Fig. 4C). Thus the differential accumulation of fat mass in wildtype and *Imp2*$^{-/-}$ mice on a HFD occurs in the absence of measureable differences in food intake per mouse (on either diet), and in the absence of fat malabsorption.

Energy expenditure (EE) was estimated at several ages using indirect calorimetry. Cohorts of males taken immediately after weaning (~4 weeks) were placed on a HFD, acclimatized to the metabolic cages and examined after ~ 4 days on the HFD (Fig. 4D): at this time the *Imp2*$^{-/-}$ males weigh slightly but significantly less than wildtype (15 gm vs 14 gm, p=0.046, Fig. 4D, upper left) a difference due entirely to a smaller lean mass (Fig.5D, upper, second from left). The RER (Fig. 4D, upper right) and absolute energy expenditures per animal were not different in *Imp2*$^{-/-}$ as compared to wild type (Fig.4D lower left). However, energy expenditure corrected for TBW (Fig. 4D, lower middle) or lean mass (Fig. 4D, lower right) was ≈ 10% higher in the *Imp2*$^{-/-}$ (p=0.01 and 0.002 respectively). Five week old female wildtype and *Imp2*$^{-/-}$ mice placed on the HFD for 4 days were also examined by indirect calorimetry (Fig. S3B) with similar findings. Given the rapid divergence in body size and composition after weaning (Fig. 1E), the increased EE seen in the 5 week old *Imp2*$^{-/-}$ male mice, measured at a time when their size and body composition most closely resembles the wildtype, provides the most reliable estimate of relative EE (Cannon and Nedergaard, 2011; Kaiyala and Schwartz, 2011), as compared with later ages (e.g., 16 weeks age, Fig. S3C) when body weight and composition have diverged further. Finally, measurements of physical activity taken during the calorimetry studies reveal no differences between *Imp2*$^{-/-}$ and wildtype mice (Fig. 4E). Thus, the substantially reduced deposition of fat in *Imp2*$^{-/-}$ mice is attributable primarily to a modest increase in energy expenditure.

Imp2$^{-/-}$ mice exhibit superior defense of core temperature

Given the evidence for increased energy expenditure, we examined thermogenesis. When maintained at room temperature (~23°C), the core body temperature of wildtype and *Imp2*$^{-/-}$ mice at 4, 7 and 20 weeks age is not different, whether on normal chow or on a high fat diet (Fig. 5A, B). To parallel the calorimetry studies, cohorts of 4 week old male wildtype and *Imp2*$^{-/-}$ mice were placed at 4°C; body temperature falls progressively in both wildtype and *Imp2*$^{-/-}$, but to a significantly greater extent in wildtype (Fig. 5B, upper). By 7 weeks age, the ability of *Imp2*$^{-/-}$ mice fed normal chow to better defend their core temperature is more pronounced (Fig. 5B, lower); core body temperature of *Imp2*$^{-/-}$ mice remains significantly higher than wildtype for the first 24 hours at 4°C. By 48 hours, however, the body temperature of knockout and wild type mice have converged (Fig. 5C).

The superior defense of core temperature in the cold-exposed *Imp2*$^{-/-}$ mice suggests a greater thermogenic response, especially in view of their smaller size/lean mass and lesser adiposity. Thermogenesis in this circumstance is due to shivering (Block, 1994), which is evident in both cohorts and generates heat though contractile activity (friction), and to catecholamine-induced activation of thermogenesis in brown fat (Cannon and Nedergaard, 2004). The latter reflects catecholamine-stimulated mitochondrial metabolism and electron transport accompanied by fatty acid activation of UCP1 (Fedorenko et.al., 2012), which dissipates the proton gradient as heat (Cannon and Nedergaard, 2011; Divakaruni and Brand, 2011).

Imp2$^{-/-}$ brown adipocytes have more UCP1 polypeptide and higher uncoupled oxygen consumption

To estimate of the relative abundance of mitochondria in brown fat and other tissues we measured the activity of Citrate Synthase (CS) and the electron transport complexes I-IV (Frazier and Thorburn, 2012) as well as the ratio of mitochondrial DNA to nuclear DNA. Whereas the ratio of mitochondrial DNA to nuclear DNA is higher in most tissues of *Imp2*$^{-/-}$ mice than in wildtype mice (Fig. 5D, left), no significant differences in the activity of CS (Fig. 5D, right) or of the electron transport complexes (Figure. S4) were detected; in addition, the level of acetylated PGC1α in brown fat does not differ between *Imp2*$^{-/-}$ and wildtype mice (Fig. S5A). Inasmuch as CS correlates much more closely with mitochondrial fractional area determined by electron microscopy than does mitochondrial DNA (Larsen et.al., 2012), these data indicate that mitochondrial oxidative capacity is not different in the *Imp2*$^{-/-}$. Nevertheless, the presence of UCP1 in BAT mitochondria directs its oxidative metabolism almost entirely to thermogenesis; we therefore examined the abundance of the UCP1 polypeptide in brown adipose tissue from wildtype and *Imp2*$^{-/-}$ mice. In five week old male wildtype and *Imp2*$^{-/-}$ mice maintained at room temperature and fed a HFD from weaning (to parallel the conditions used for calorimetry) the UCP1 polypeptide content of the *Imp2*$^{-/-}$ BAT is modestly but significantly greater than wildtype (Fig. 5E), whereas the abundance of Ucp1 mRNA does not differ (Fig. S5B). In sixteen week old mice maintained at room temperature on NCD, The UCP1 polypeptide in brown fat was also approximately two fold more abundant in the *Imp2*$^{-/-}$ mice than in wildtype. Moreover, the increase in UCP1 protein abundance upon residence at 4°C for 72 hours is much more pronounced in the *Imp2*$^{-/-}$ mice than in wildtype (Fig. 5F). In contrast to the differences in UCP1 polypeptide abundance in wildtype and *Imp2*$^{-/-}$ brown fat, the level of *Ucp1* mRNA in brown fat, whether measured by QPCR (Fig. S5C; Table S3) or by deep sequencing (Table S4), although increased markedly in both genotypes by cold exposure, is not different in the wildtype as compared with *Imp2*$^{-/-}$ mice. Notably, cold exposure reduces the abundance of IMP2 in the brown fat of wildtype mice by nearly 70% (Fig. 5G).

We sought to determine whether the metabolic activity of brown fat was increased in the *Imp2*$^{-/-}$. Measurements of ^{18}F-FDG uptake in vivo into the interscapular brown fat of cold exposed mice (Fig.S6A) and of norepinephrine-stimulated oxygen consumption in vitro by primary brown adipocytes isolated from interscapular BAT (Fig.S6B) each gave highly variable results that did not reveal significantly different responses between wildtype and *Imp2*$^{-/-}$. We next examined oxygen consumption by stromal vascular cells isolated from

interscapular brown fat pads (Klein et.al. 1999) and differentiated into brown adipocytes in vitro (Kajimura et.al., 2009) (Fig. 5H-J). The extent of differentiation was comparable for SVCs isolated from the BAT of *Imp2*$^{+/+}$ and *Imp2*$^{-/-}$ mice, as judged by staining with oil-red-O and by the abundance of a cohort of differentiation-dependent mRNAs (Fig. 5H). Despite the similar *Ucp1* mRNA levels, the abundance of the UCP1 polypeptide in the *Imp2*$^{-/-}$ brown adipocytes obtained by differentiation in vitro was approximately two-fold higher than wildtype (Fig. 5I), as had been observed in interscapular BAT (Fig. 5E). Overall oxygen consumption by the *Imp2*$^{-/-}$ brown adipocytes differentiated in vitro (Fig. 5J) was significantly greater than that of *Imp2*$^{+/+}$ brown adipocytes; pretreatment of the cells with isoproterenol increased the oxygen consumption of all cells but enlarged the difference between *Imp2*$^{-/-}$ and *Imp2*$^{+/+}$ adipocytes. In the presence of oligomycin, the rate of uncoupled oxygen consumption was approximately two-fold greater in the *Imp2*$^{-/-}$ adipocytes than in *Imp2*$^{+/+}$ cells. These results support the conclusion that the increased abundance of UCP1 polypeptide in *Imp2*$^{-/-}$ BAT is an integral feature of brown fat differentiation in the absence of *Imp2*$^{-/-}$. Moreover, they demonstrate that the increased abundance of UCP1 polypeptide is accompanied by an increase in uncoupled oxygen consumption.

IMP2 binds *Ucp1* mRNA and suppresses its translation

Given the higher UCP1 polypeptide abundance in *Imp2*$^{-/-}$ vs wildtype brown fat without differences in *Ucp1 mRNA* abundance, we hypothesized that IMP2, a known translational regulator, might regulate translation of *Ucp1* mRNA. Anti-IMP2 immunoprecipitates were prepared from wildtype and *Imp2*$^{-/-}$ brown fat, as well from wildtype brown fat using anti-IMP2 and non-immune IgG (Fig. 6A). The *Ucp1* mRNA was specifically associated with IMP2 using qPCR (Table S3) as well as RNA sequencing. In RNA sequencing data we identified 83 RNAs that exhibit greater than 1.5 fold enrichment in IMP2 immunoprecipitates (Fig. 6A and Table S4); over 40% of these candidate IMP2 clients encode mitochondrial components, including *Ucp1*, (Fig. 6B, Table S5).

Seeking independent confirmation, we used QPCR to estimate the abundance of the top 21 of these 83 candidate IMP2 partner mRNAs, using as input total and anti-IMP2-bound RNAs from wildtype and *Imp2*$^{-/-}$ brown fat. Of the 21, 15 (71%) were confirmed to be enriched in the IMP2 IP from wildtype BAT (Fig. 6C, upper). Note that the total mRNA abundance for 14 of these 15 candidates, including *Ucp1* is unaltered by elimination of IMP2 (Fig. 6C, lower).

To evaluate whether the absence of IMP2 altered the translation of the candidate IMP2 client mRNAs, we prepared postnuclear extracts of wildtype and *Imp2*$^{-/-}$ brown fat. These extracts were separated by sucrose density gradient centrifugation and the fraction of mRNAs comigrating with polysomes measured by QPCR both for *Gapdh* (as a control) and of each of the 21 candidate IMP2 clients (Fig. 6D). Among the fifteen QPCR-confirmed IMP2 client mRNAs, thirteen — including *Ucp1* — show a significantly higher fractional polysomal abundance the *Imp2*$^{-/-}$ extracts (Fig. 6D). All thirteen encode mitochondrial components.

To directly test the effect of IMP2 on the translation of *Ucp1* mRNA, we flanked the coding sequences of firefly Luciferase with the 5' and 3'UTR of murine *Ucp1* mRNA, as well as with several control UTRs. These controls included the 5'UTRs of human beta globin and the human *IGF2* leader 3 (L3) and leader 4 (L4). It has previously been shown that IMP2 does not bind to the beta globin or *IGF2L4* 5'UTRs, but binds to the *IGF2L3* 5'UTR and enables translation of this mRNA by internal ribosomal entry (Dai et.al., 2011). The in vitro transcribed RNAs were used to program reticulocyte lysates and their translation was monitored by the level of Luciferase enzyme activity in the relation to increasing amounts of recombinant Flag-IMP2.

As expected, IMP2 does not alter the translation of Luciferase mRNAs bearing generic UTRs or the beta globin or *IGF2L4* 5'UTRs. As before, IMP2 causes a dose dependent stimulation of *IGF2L3*-Luciferase mRNA. In contrast, addition of IMP2 causes a progressive inhibition of *Ucp1*-Luciferase mRNA translation (Fig. 6E)

In summary, IMP2 binds many mRNAs encoding mitochondrial components both *in vivo* and *in vitro*, and restrains their steady state rate of translation. These data support the hypothesis that in the absence of IMP2, loss of translational inhibition leads to a higher steady state level of UCP1 polypeptide in the brown fat, and this modest but sustained increase in UCP1 abundance contributes to the higher energy expenditure and resistance to diet induced obesity

Discussion

The phenotype of the *Imp2*$^{-/-}$ mice includes: 1) modestly smaller size, with slightly diminished linear growth and less accrual of lean mass after weaning; 2) when fed a high fat diet, much less fat in white adipose depots despite similar food intake, fat absorption and physical activity; 3) smaller white adipose depots containing fewer adipocyte precursors and fewer mature fat cells of equal size to those in obese wildtype littermate; 4) modestly increased energy expenditure; 5) improved glucose tolerance, insulin sensitivity and resistance to the development of fatty liver; and 6) substantially longer lifespan. *Imp2*$^{+/-}$ mice did not exhibit smaller size or resistance to diet induced obesity and the median survival of small cohort (10 males+10 females) did not differ from that of the wildtype mice in Fig. 1G.

The best explanation we could identify for the differential gain of the *Imp2*$^{-/-}$ mice in fat mass, both on normal chow and the high fat diet, is increased energy expenditure as measured by indirect calorimetry. As regard the source of increased energy expenditure in the *Imp2*$^{-/-}$ mice, the lesser initial fall in their core temperature consistently observed when exposed to 4°C provides an important clue. Mice maintained at 22–23°C, far from their thermoneutral temperature (28–30°C), are partially cold adapted, a response that involves increased mitochondrial biogenesis and UCP1 expression in brown fat (Cannon and Nedergaard, 2004, 2011). *Imp2*$^{-/-}$ mice maintained at 23°C exhibit a modestly increased mitochondrial DNA content in most major tissues, however the activities of Citrate Synthase and electron transport complexes I-IV do not differ, indicating that maximal oxidative capacity is unaltered. Nevertheless, the BAT of *Imp2*$^{-/-}$ mice contains ~2 fold higher

content of UCP1 polypeptide than the wildtype; thus despite the unaltered electron transport capacity, the greater abundance of UCP1 enables a greater proton leak at any level of electron transport and is likely to account for the greater ability of the *Imp2*$^{-/-}$ mice to defend their core temperature in response to the catecholamine surge engendered by cold exposure. Interestingly, UCP1 levels in in *Imp2*$^{-/-}$ subcutaneous white fat appear diminished; this eliminates "browning" of white fat as the source of the increased energy expenditure.

The mechanism underlying the increased abundance of UCP1 in *Imp2*$^{-/-}$ brown fat is post-transcriptional, inasmuch as IMP2 deficiency does not alter *Ucp1* mRNA abundance. Rather, IMP2 binds *Ucp1* mRNA specifically in brown fat and, as reflected by fractional polysomal abundance, elimination of IMP2 enhances the translational efficiency of *Ucp1* mRNA. IMP2 specifically inhibits *Ucp1* mRNA translation in vitro, by binding to untranslated segments; thus, the improved translational efficiency of *Ucp1* mRNA in IMP2 deficient-brown fat is, at least in part, directly attributable to the elimination of IMP2. This increase in translational efficiency is also likely to account for why, when mice are exposed to 4°C, the abundance of UCP1 polypeptide increases more rapidly in *Imp2*$^{-/-}$ brown fat, despite comparable levels of *Ucp1* mRNA.

Several features point to a more complex role for IMP2 in mitochondrial biogenesis and function beyond the control of *Ucp1* mRNA translation. These include the widespread increase in mitochondrial DNA and the enhanced translational efficiency of many BAT mRNAs encoding mitochondrial electron transport components in *Imp2*$^{-/-}$ BAT, occurring without alteration in the enzymatic activity of the BAT electron transport complexes. In preliminary studies, we have observed that mitochondrial DNA is also increased in *Imp2*$^{-/-}$ (but not *Imp1*$^{-/-}$) MEFs, whereas maximal oxygen consumption is actually reduced by 50%, suggesting that the increased mitochondrial DNA may be a compensatory response. These findings are consistent with the report of Janiszewska et.al., (2012) who also observed that IMP2 binds mRNAs encoding electron transport components and that shRNAs directed at *Imp2* resulted in a decrease in the activity of Complex I and IV. Thus we speculate that IMP2, in addition to controlling the translation of some mitochondrial mRNAs, may also be required for the transport of these mRNAs to the vicinity of mitochondria, where their localized translation could facilitate cotranslational mitochondrial uptake, as occurs in yeast (Weis et.al., 2013). Such a function would be analogous to IMP1, which in addition to its stimulatory role in IGF2 translation (Dai et.al., 2013), also binds beta actin mRNA, silencing its translation and mediating its transport to the cell periphery, where it is released consequent to IMP1 phosphorylation by cSrc (Hüttelmaier et.al., 2005).

As to the basis for the prolonged lifespan of the *Imp2*$^{-/-}$ mice, we speculate that increased energy expenditure is a likely contributor: several other mouse models with sustained increases in energy expenditure also exhibit a lean, obesity-resistant phenotype and prolonged lifespan (e.g., inactivation of *Rps6kb1*(Selman et.al., 2009), transgenic expression of UCP1 in skeletal muscle (Gates et.al., 2007), low dose treatment with 2,4 dinitrophenol (Caldeira da Silva et.al., 2008). In addition, the presence of malignancies in 4/6 healthy but aged wildtype mice together with the lack of detectable malignancy in six *Imp2*$^{-/-}$ littermates raises the possibility that the lack of the oncofetal protein and cancer biomarker

IMP2 (Kessler et.al., 2013) is protective against carcinogenesis. Among the diverse array of genetic alterations known to extend lifespan in mice (Chen et.al., 2010; Selman and Withers, 2011) are several loss-of-function mutations in the growth hormone and IGF1 axis; although the *Imp2*$^{-/-}$ mice show diminished growth especially post-weaning, serum levels of IGF1 during and after maximal growth and levels of IGFBPs 1 and 3 are not different from wildtype.

We also note that IMP2 is a rapamycin-sensitive substrate for mTORC1 (Dai et.al., 2011) and is also phosphorylated by mTORC2 (Dai et.al., unpublished). Rapamycin treatment (Harrison et.al., 2009) and hypomorphic mutation of the *mTOR* gene in mice each (Wu et.al., 2013) prolongs lifespan. Whether this occurs by delay of senescent phenotypes or by reduced carcinogenesis (or both) is uncertain (Wilkinson et.al., 2012). It will thus be of interest to test whether IMP2 is contributory to the extension of lifespan engendered by inhibition or deficiency of mTOR complex 1, and whether mTOR phosphorylation of IMP2 is important to its lifespan-related actions.

A strong impetus to the investigation of the physiologic roles of IMP2 is the presence in the human *IMP2* gene of SNPs in intron 2 that confer increased risk for Type 2 diabetes and alterations in insulin secretion (Groenewoud et.al.,2008), the beta cell (Marselli et.al., 2010) and insulin resistance (e.g., Li et.al., 2009). These SNPs are noncoding and insufficient to prove that *IMP2* is the causal gene in the linked region. Our finding of substantial metabolic and glycemic phenotypes in the *Imp2*$^{-/-}$ mice supports the case for *IMP2* as the causal gene. The demonstration that IMP2 controls the translation of mitochondrial mRNAs and possibly mitochondrial biogenesis focuses further efforts to understand the role of IMP2 to a domain of energy metabolism known to be important to both insulin secretion and insulin action in the periphery and to be altered in human Type 2 diabetes.

Experimental Procedures

Generation of the *Imp2* targeting construct

The construct was generated by using a genomic fragment of 12 kb containing *Imp2* exon 1 and 2 as well as flanking intron sequences of the murine gene extracted from the RP23-163F16 BAC clone. The replacement-type targeting construct consisted of 9.4 kb of *Imp2* genomic sequences (4.4 kb in the left homology arm (5') and 5.4 kb in the right homology arm (3')). (Fig. S1).

Whole Animal studies

Animals used for experiments are bred by *Imp2* +/−;*Imp2* +/− mating. *Imp2*−/− mice and wild-type littermates were maintained on C57Bl/6J background in a specific pathogenfree facility with 12:12 light:dark cycle, and fed irradiated chow (Prolab 5P75 Isopro 3000; 5% crude fat; PMI nutrition international) or a high fat diet (D12492i; 60kca%l fat; Research Diets Inc.). Body composition was evaluated in live, conscious animals in triplicate by quantitative nuclear magnetic resonance spectroscopy (EchoMRI Analyzer; Echo Medical Systems, Houston, TX). After mice had acclimated in individually housed metabolic cages for 3 days, measurements of energy expenditure, food intake and physical activity were

performed using an indirect calorimetric system (TSE Labmaster, 17826 Edison Avenue Chesterfield, MO 63005). Glucose tolerance was measured after a 14 hr fast by IP injection of glucose (1g/ kg); insulin tolerance was estimated after IP injection of insulin (0.4U/kg) after a 5 hour fast. Body temperature was measured a Physitemp BAT-12 rectal probe.

Brown fat studies

The stromal vascular compartment was isolated from interscapular brown fat, grown to confluence and differentiated to brown adipocytes according to Kajimura et.al. (2009) by incubation with isobuylmethylxanthine (0.5mM), dexamethasone (1uM), insulin (17nM), rosiglitazone (1uM) and T3 (1nM). After 48h the medium was changed to contain insulin (17nM) and rosiglitazone (1uM); two days later rosiglitazone was removed and two days thereafter insulin was reduced to 850nM. Measurements of total respiration by cell suspensions were taken in a Clark electrode (Strahkelvin Instruments) before and after the addition of oligomycin (1μM), and normalized for protein content. For IMP2 IP from BAT, tissue was extracted for 10 min with tissue lyser (Qiagene) in ice cold lysis buffer (140 mM KCl, 1.5 mM MgCl2, 20 mM Tris-HCl at pH 7.4, 0.5% Nonidet P-40, 0.5 mM dithiothreitol, 1 U/μL RNase inhibitor, one complete EDTA-free protease inhibitor cocktail tablet). The lysate was centrifuged for 10 min at 14,000rpm; IMP2 IP and RNA extraction was performed as in Dai et.al. (2011). For analysis of BAT polysomes, the lysis buffer also contained 150 mg/mL cycloheximide, 1000U/ml RNase inhibitor (Roche diagnostics) and 40mM vanadyl-ribonucleoside complex (NEB). Sucrose density gradient separation of polysomes and in vitro translation in the presence of recombinant Flag-IMP2 were performed as before (Dai et.al., (2013).

RNA analyses

Total RNA was isolated using the Trizol reagent and Qiagene RNase kit (Qiagen). RNA samples were examined for the integrity by Agilent bioanalyzer prior to real time PCR (see Table S6 for primers) or short-fragment library construction for Illumina sequencing (MGH next generation sequencing core). Raw sequence FASTQ files were aligned to the Mus Musculus genome version 10 (mm10) using Tophat version 2.0.8 (http://tophat.cbcb.umd.edu) calling Bowtie version 2.1.0 (http://bowtiebio.sourceforge.net/bowtie2/manual.shtml) and SAMtools version 0.1.18 (http://samtools.sourceforge.net/). Resulting BAM files were quality tested using RNASeQC version 1.1.7 (http://www.broadinstitute.org/cancer/cga/rna-seqc). Transcript assembly, abundance estimation and differential expression were performed using Cufflinks/Cuffdiff version 2.1.1 (http://cufflinks.cbcb.umd.edu/). Cuffdiff output files used for subsequent analyses were pruned to include only genes with status OK and exclude genes with fold change or test statistic approaching infinity. RNA sequence data from liver (Fig.2E), brown fat and IMP2 IPs are accessible at GEO (to be provided).

Enzyme and other assays

Citrate Synthase was determined as in Frazier and Thorburn (2012). Immunoblots were performed as in Dai et.al. (2011), The ratio of nuclear and mitochondrial DNA was quantitated by real-time PCR (Table S6).

Statistical Analysis

Comparisons between the mean±s.e.m or s.d of two groups were calculated using twoway ANOVA or Student's unpaired 2-tailed t test. P values of 0.05 or less were considered statistically significant.

Supplementary Material

Refer to Web version on PubMed Central for supplementary material.

Acknowledgements

Supported by NIH awards R37DK17776 (JA), P30DK057521 (JA) the Instituto Carso de la Salud, A.C. via the Slim Initiative in Genomic Medicine for the Americas (DA) and institutional funds. DK and LM thank the EMBL-Monterotondo gene expression and transgenic services for the production of the *Imp2*$^{-/-}$ line. LM was supported in part by the Lundbeck foundation (grant 177/05). DK was supported by an EMBL-postdoctoral fellowship; DRT by an NHMRC Principal Research Fellowship. We thank Evan Rosen, Paul Cohen, Bruce Spiegelman, Youn-Kyoung Lee, Chad Cowan, Gerald I. Shulman, Alex Soukas and Finn C. Nielsen for discussions, Paul Cohen and Youn-Kyoung for preliminary experiments, O. Peroni for adipocyte size determination and A. Laskowski and T. Stait for technical assistance.

References

Block BA. Thermogenesis in muscle. Annu Rev Physiol. 1994; 56:535–577. [PubMed: 8010751]

Caldeira da Silva CC, Cerqueira FM, Barbosa LF, Medeiros MH, Kowaltowski AJ. Mild mitochondrial uncoupling in mice affects energy metabolism, redox balance and longevity. Aging Cell. 2008; 7:552–560. [PubMed: 18505478]

Cannon B1, Nedergaard J. Brown adipose tissue: function and physiological significance. Physiol Rev. 2004; 84:277–359. [PubMed: 14715917]

Cannon B, Nedergaard J. Nonshivering thermogenesis and its adequate measurement in metabolic studies. J Exp Biol. 2011; 214(Pt 2):242–253. [PubMed: 21177944]

Chen YF, Wu CY, Kao CH, Tsai TF. Longevity and lifespan control in mammals: lessons from the mouse. Ageing Res Rev. 2010; 9(Suppl 1):S28–S35. [PubMed: 20667513]

Colditz GA, Willett WC, Rotnitzky A, Manson JE. Weight gain as a risk factor for clinical diabetes mellitus in women. Ann Intern Med. 1995; 122:481–486. [PubMed: 7872581]

Dai N, Rapley J, Angel M, Yanik MF, Blower MD, Avruch J. mTOR phosphorylates IMP2 to promote IGF2 mRNA translation by internal ribosomal entry. Genes Dev. 2011; 25:1159–1172. [PubMed: 21576258]

Dai N, Christiansen J, Nielsen FC, Avruch J. mTOR Complex 2 phosphorylates IMP1 cotranslationally to promote IGF2 production and the proliferation of mouse embryonic fibroblasts. Genes Dev. 2013; 27:301–312. [PubMed: 23388827]

DIAbetes Genetics Replication And Meta-analysis (DIAGRAM) Consortium. Genome wide trans-ancestry meta-analysis provides insight into the genetic architecture of type 2 diabetes. Nat. Genet. 2014; 2:34–44.

Divakaruni AS, Brand MD. The regulation and physiology of mitochondrial proton leak. Physiology (Bethesda). 2011; 3:192–205. [PubMed: 21670165]

Fedorenko A1, Lishko PV, Kirichok Y. Mechanism of fatty-acid-dependent UCP1 uncoupling in brown fat mitochondria. Cell. 2012; 151:400–413. [PubMed: 23063128]

Frazier AE, Thorburn DR. Biochemical analyses of the electron transport chain complexes by spectrophotometry. Methods in Mol Biol. 2012; 837:49–62. [PubMed: 22215540]

Gates AC1, Bernal-Mizrachi C, Chinault SL, Feng C, Schneider JG, Coleman T, Malone JP, Townsend RR, Chakravarthy MV, Semenkovich CF. Respiratory uncoupling in skeletal muscle delays death and diminishes age-related disease. Cell Metab. 2007; 6:497–505. [PubMed: 18054318]

Groenewoud MJ, Dekker JM, Fritsche A, Reiling E, Nijpels G, Heine RJ, Maassen JA, Machicao F, Schäfer SA, Häring HU, 't Hart LM, van Haeften TW. Variants of CDKAL1 and IGF2BP2 affect first-phase insulin secretion during hyperglycaemic clamps. Diabetologia. 2008; 51:1659–1663. [PubMed: 18618095]

Harrison DE, Strong R, Sharp ZD, Nelson JF, Astle CM, Flurkey K, Nadon NL, Wilkinson JE, Frenkel K, Carter CS. Rapamycin fed late in life extends lifespan in genetically heterogeneous mice. Nature. 2009; 460:392–395. [PubMed: 19587680]

Janiszewska M, Suvà ML, Riggi N, Houtkooper RH, Auwerx J, Clément-Schatlo V, Radovanovic I, Rheinbay E, Provero P, Stamenkovic I. IMP2 controls oxidative phosphorylation and is crucial for preserving glioblastoma cancer stem cells. Genes Dev. 2012; 26:1926–1944. [PubMed: 22899010]

Kajimura S, Seale P, Kubota K, Lunsford E, Frangioni JV, Gygi SP, Spiegelman BM. Initiation of myoblast to brown fat switch by a PRDM16-C/EBP-beta transcriptional complex. Nature. 2009; 460:1154–1158. [PubMed: 19641492]

Kaiyala KJ, Schwartz MW. Toward a more complete (and less controversial) understanding of energy expenditure and its role in obesity pathogenesis. Diabetes. 2011; 60:17–23. [PubMed: 21193735]

Kessler SM, Pokorny J, Zimmer V, Laggai S, Lammert F, Bohle RM, Kiemer AK. IGF2 mRNA binding protein p62/IMP2-2 in hepatocellular carcinoma: antiapoptotic action is independent of IGF2/PI3K signaling. Am J Physiol Gastrointest Liver Physiol. 2013; 304:G328–G336. [PubMed: 23257922]

Knowler WC, Barrett-Connor E, Fowler SE, Hamman RF, Lachin JM, Walker EA, Nathan DM. Diabetes Prevention Program Research Group. Reduction in the incidence of type 2 diabetes with lifestyle intervention or metformin. N Engl J Med. 2002; 346:393–403. [PubMed: 11832527]

Larsen S, Nielsen J, Niegaard-Hansen C, Nielsen LB, Wibrand F, Stride N, Schrodder HD, Boushel R, Helge JW, Dela F, Hey-Mogensen M. Biomarkers of mitochondrial content in skeletal muscle of healthy young human subjects. J Physiol. 2012; 590:3349–3360. [PubMed: 22586215]

Li X, Allayee H, Xiang AH, Trigo E, Hartiala J, Lawrence JM, Buchanan TA, Watanabe RM. Variation in IGF2BP2 interacts with adiposity to alter insulin sensitivity in Mexican Americans. Obesity (Silver Spring). 2009; 17:729–376. [PubMed: 19148120]

Marselli L, Thorne J, Dahiya S, Sgroi DC, Sharma A, Bonner-Weir S, Marchetti P, Weir GC. Gene expression profiles of Beta-cell enriched tissue obtained by laser capture microdissection from subjects with type 2 diabetes. PLoS One. 2010; 5:e11499. [PubMed: 20644627]

Nielsen J, Christiansen J, Lykke-Andersen J, Johnsen AH, Wewer UM, Nielsen FC. A family of insulin-like growth factor II mRNA-binding proteins represses translation in late development. Mol Cell Biol. 1999; 19:1262–1270. [PubMed: 9891060]

Rodeheffer MS, Birsoy K, Friedman JM. Identification of white adipocyte progenitor cells in vivo. Cell. 2008; 135:240–249. [PubMed: 18835024]

Saxena R, Voight BF, Lyssenko V, Burtt NP, de Bakker PI, Chen H, Roix JJ, Kathiresan S, Hirschhorn JN, Daly MJ. Genome-wide association analysis identifies loci for type 2 diabetes and triglyceride levels. Diabetes Genetics Initiative of Broad Institute of Harvard and MIT, Lund University, and Novartis Institutes of BioMedical Research, Science. 2007; 316:1331–1336. [PubMed: 17463246]

Scott LJ, Mohlke KL, Bonnycastle LL, Willer CJ, Li Y, Duren WL, Erdos MR, Stringham HM, Chines PS, Jackson AU. A genome-wide association study of type 2 diabetes in Finns detects multiple susceptibility variants. Science. 2007; 316:1341–1345. [PubMed: 17463248]

Selman C, Tullet JM, Wieser D, Irvine E, Lingard SJ, Choudhury AI, Claret M, Al-Qassab H, Carmignac D, Ramadani F. Ribosomal protein S6 kinase 1 signaling regulates mammalian life span. Science. 2009; 326:140–144. [PubMed: 19797661]

Selman C, Withers DJ. Mammalian models of extended healthy lifespan. Philos Trans R Soc Lond B Biol Sci. 2011; 366:99–107. [PubMed: 21115536]

Turturro A, Duffy, Hass B, Kodell R, Hart R. Survival characteristics and Age-adjusted disease incidences in C57BL/6 fed a commonly used cereal-based diet modulated by dietary restriction. J Gerontol A Biol Sci Med Sci. 2002; 57:B379–B389. [PubMed: 12403793]

Tybl E, Shi FD, Kessler SM, Tierling S, Walter J, Bohle RM, Wieland S, Zhang J, Tan EM, Kiemer AK. Overexpression of the IGF2-mRNA binding protein p62 in transgenic mice induces a steatotic phenotype. J Hepatol. 2011; 54:994–1001. [PubMed: 21145819]

Wang C, Li Q, Redden DT, Weindruch R, Allison DB. Statistical methods for testing effects on "maximum lifespan". Mech Aging Dev. 2004; 125:629–632. [PubMed: 15491681]

Weiss BL, Schlieff E, Zerges W. Protein targeting to subcellular organelles via mRNA localization. Biochim Biophys Acta. 2013; 1833:260–273. [PubMed: 23457718]

Wilkinson JE, Burmeister L, Brooks SV, Chan CC, Friedline S, Harrison DE, Hejtmancik JF, Nadon N, Strong R, Wood LK, Woodward MA, Miller RA. Rapamycin slows aging in mice. Aging Cell. 2012; 11:675–682. [PubMed: 22587563]

Wu JJ, Liu J, Chen EB, Wang JJ, Cao L, Narayan N, Fergusson MM, Rovira II, Allen M, Springer DA, Lago CU, Zhang S, DuBois W, Ward T, deCabo R, Gavrilova O, Mock B, Finkel T. Increased mammalian lifespan and a segmental and tissue-specific slowing of aging after genetic reduction of mTOR expression. Cell Rep. 2013; 4:913–920. [PubMed: 23994476]

Yisraeli JK. VICKZ proteins: a multi-talented family of regulatory RNA-binding proteins. Biol Cell. 2005; 97:87–96. [PubMed: 15601260]

Zeggini E, Weedon MN, Lindgren CM, Frayling TM, Elliott KS, Lango H, Timpson NJ, Perry JR, Rayner NW, Freathy RM, Wellcome Trust Case Control Consortium (WTCCC). McCarthy MI, Hattersley AT. Replication of genome-wide association signals in UK samples reveals risk loci for type 2 diabetes. Science. 2007; 316:1336–1341. [PubMed: 17463249]

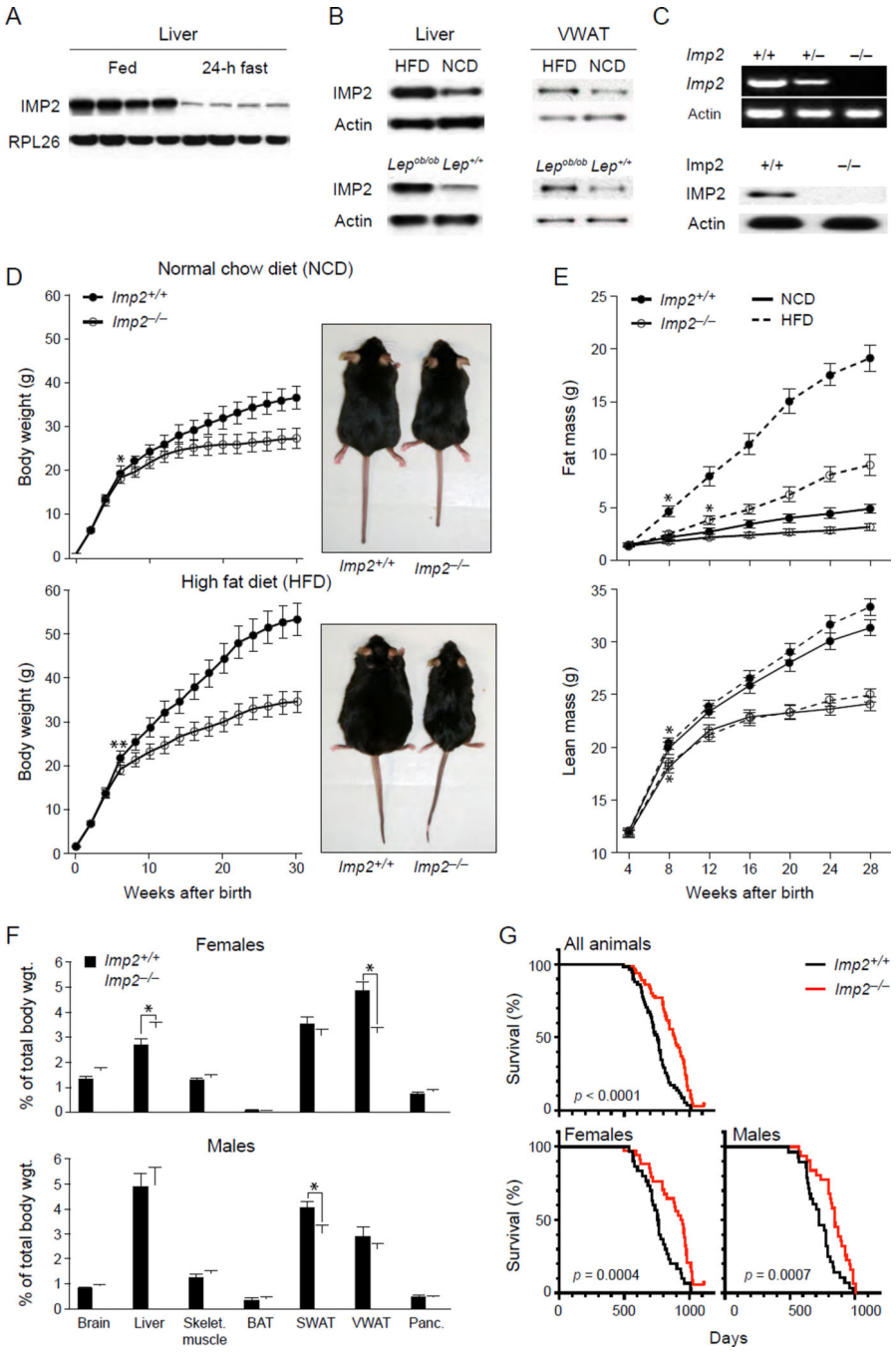

Figure 1. IMP2 affects postnatal growth, response to fat feeding and lifespan

A) Fasting reduces IMP2 polypeptide in Liver. Four pairs of male mice 12 weeks age maintained on normal chow were deprived of food for 24 hrs prior to sacrifice.

B) IMP2 abundance in liver and WAT is increased by HFD and in obesity. Upper: six week old C57Bl6 male mice were fed a HFD for one week and sacrificed; Lower: six week old male *Lep*$^{ob/ob}$ mice and wildtype littermates on NCD; extracts of liver and gonadal fat were immunoblotted for IMP2 and actin.

C) *Imp2* mRNA and protein expression in mouse embryos. Extracts of wildtype and Imp2 knockout mouse embryos at E12.5 were analyzed for *Imp2* and *actin* mRNA (upper) and protein (lower).

D) Growth curves of wildtype and *Imp2*$^{-/-}$ male mice on normal chow and HFD. Upper: Growth curves on normal chow of wildtype and *Imp2*$^{-/-}$ male mice; error bars=1 S.D. Body weight is not different at 4 weeks (weaning) but is significantly greater in the wildtype at 6 weeks and at all times thereafter (*=p<0.05). Right: 30 week old wildtype and *Imp2*$^{-/-}$ female mice maintained on NCD.

Lower: Growth curves on a HFD from 4 weeks age; weight is not different at 4 weeks but is significantly greater in the wildtype at 6 weeks age (**=p<0.001) and thereafter. Right: 30 week old wildtype and *Imp2*$^{-/-}$ female mice maintained on a HFD from weaning.

E) Effect of IMP2 deficiency on body composition. Upper: Fat mass of wildtype (filled circles) and *Imp2*$^{-/-}$ (open circles) mice on NCD (solid line) and HFD (dashed line), as estimated by MRI; error bar=1S.D. On the NCD, the fat mass in the wildtype is not greater than the *Imp2*$^{-/-}$ until 12 weeks age (*=p<0.01); on the HFD, the fat mass of the wildtype is larger at 8 weeks age (*=p<0.01). Lower: Lean mass of wildtype (filled circles) and *Imp2*$^{-/-}$ (open circles) mice on NCD (solid lines) and HFD, (dashed lines). Lean mass is not different until 8 weeks age on both diets (*,*=p<0.01).

F) Selected organ weights of wildtype (black bars) and *Imp2*$^{-/-}$ (white bars) mice maintained on a HFD from weaning, expressed as % of TBW (*=p<0.05). The upper graph summarizes results from 12 pairs of females 30 weeks age. The lower graph shows results from eight pairs of males, 32 weeks age. Skeletal muscle is sum of 4 hindlimb muscles (gastrocnemius, soleus, EDL and tibialis anterior), subcutaneous fat is the weight of the bilateral inguinal depots.

G) Percent survival of wildtype (black) and *Imp2*$^{-/-}$ mice (red) maintained on normal chow. The upper plot includes all animals; Median survival, *Imp2*$^{-/-}$ > wildtype, p<0.0001; the lower plots show females (30 *Imp2*$^{+/+}$ and 34 *Imp2*$^{-/-}$) on the left (p<0.0005) and males (28 *Imp*$^{+/+}$ and 31 *Imp2*$^{-/-}$)on the right (p<0.001).

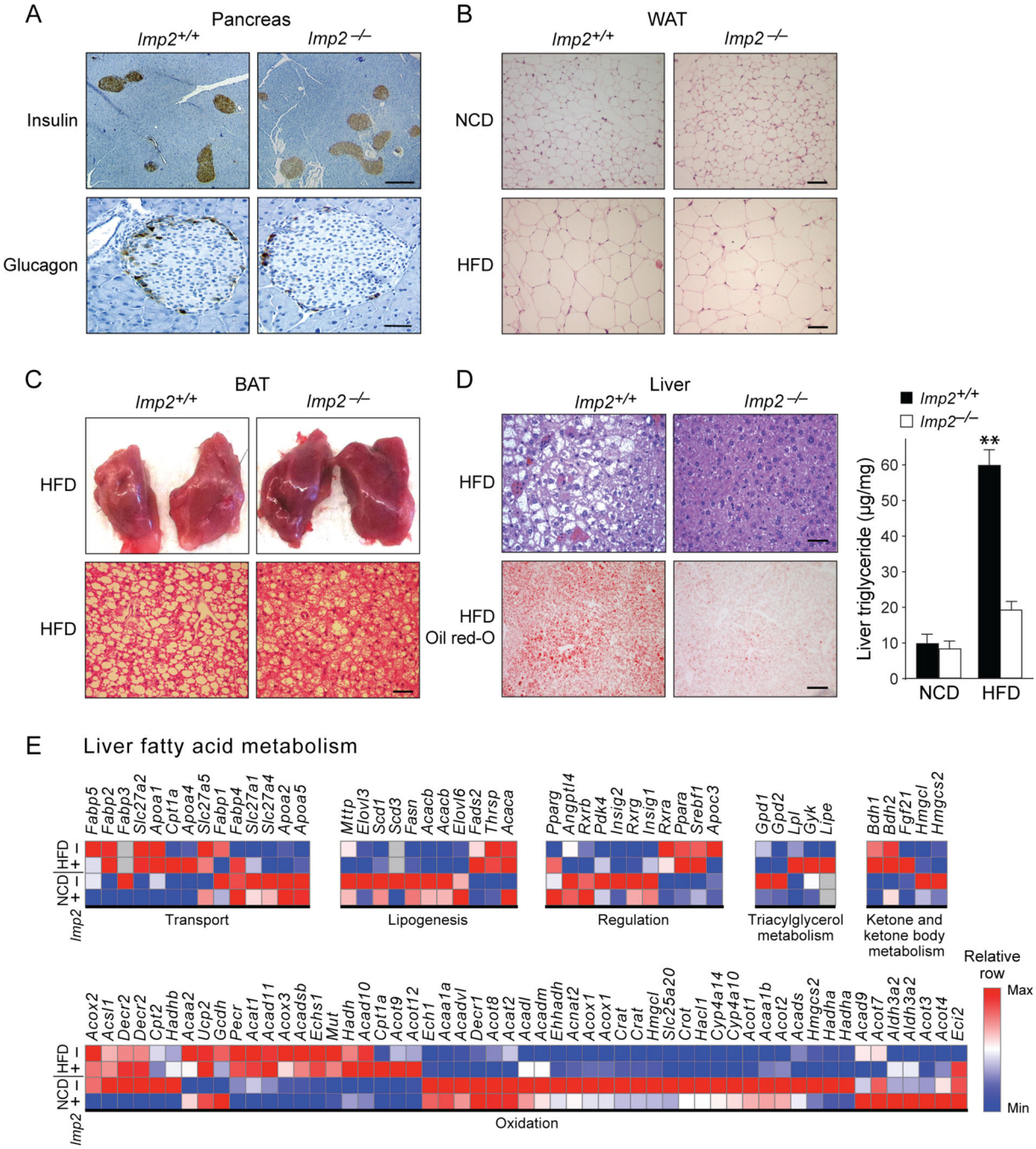

Figure 2. Histology of selected organs, liver triglyceride content and gene expression on NCD and HFD

A) Representative images of pancreatic islets from 19 week old male mice maintained on HFD from weaning, stained for insulin (upper; scale bar=250μm) and glucagon (lower; scale bar=50μm).

B) Gonadal adipose tissue of 12 week old male wildtype and *Imp2*$^{-/-}$ mice maintained on normal chow (upper) and HFD from weaning (lower); scale bar=50μM. See Fig. S2.

C) Interscapular brown adipose tissue from 12 week old male wildtype and *Imp2*$^{-/-}$ mice maintained on a HFD from weaning. Upper: gross appearance of the depot from wildtype (left) and *Imp2*$^{-/-}$ mice (right). The photomicrographs show H&E stains of tissue sections of BAT; the scale bar=50μm.

D) Liver fat content on a HFD. Upper left: liver from 19 week old wildtype and *Imp2*$^{-/-}$ male mice maintained on HFD, stained with H&E (scale bar=250 μm). Left lower: liver from 12 week old wildtype and *Imp2*$^{-/-}$ male mice maintained on HFD stained with oil red-O (scale bar=100 μM). Right: Liver triglyceride content of 16 week old wildtype (black) and *Imp2*$^{-/-}$ (white) male mice maintained on NCD (3 pairs) or HFD (3 pairs) from weaning; **p=<0.01.

E) Relative abundance of liver mRNAs encoding genes relevant to fat metabolism. *Imp2*$^{+/+}$ and *Imp2*$^{-/-}$ mice were weaned onto normal chow or a HFD and sacrificed one week later.

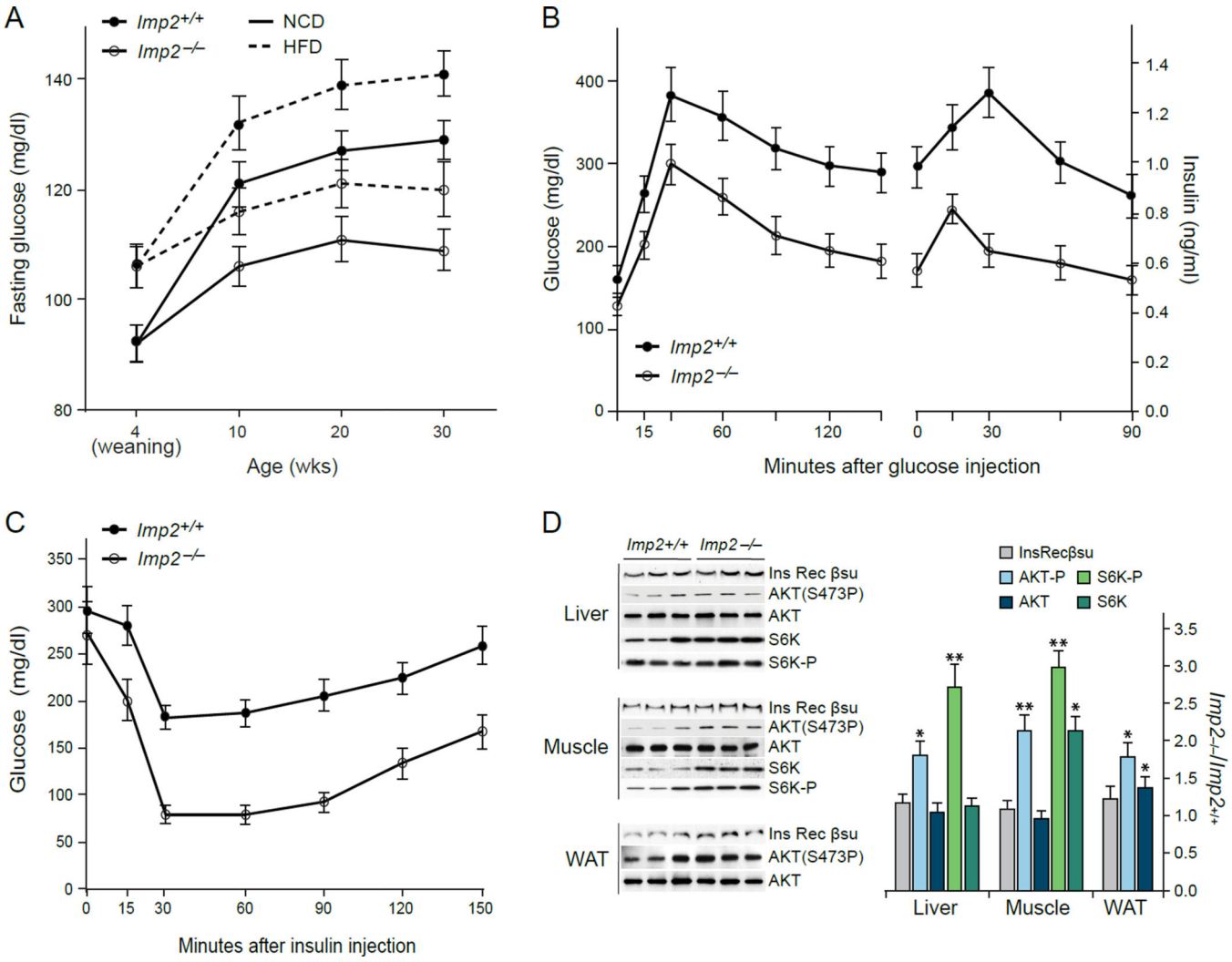

Figure 3. Glucose and insulin responses in wildtype and *Imp2*$^{-/-}$ mice

A) Fasting blood glucose with age. Blood glucose (+/− 1 S.D.) measured after ON fast in wildtype (filled circles) and *Imp2*$^{-/-}$ (open circles) mice on NCD (solid line; n=8 each genotype) and HFD (dashed line; n=8 each genotype). Values for fasting glucose are significantly different (at least $p<0.05$) between wildtype and *Imp2*$^{-/-}$ at all times after 4 weeks (weaning) on both diets.

B) Glucose tolerance tests. Glucose, 1 g/kg was administered intraperitoneally after 14 hr fasting, in 12 week old wildtype (filled circles; n=8) and *Imp2*$^{-/-}$ (open circles; n=8) male mice maintained on HFD. The glucose (+/− 1 S.D.) and insulin (+/− 1 SEM) values are significantly different (respectively, $p<0.05$ or less and $p<0.01$) at all times.

C) Insulin tolerance tests. Insulin, 0.4U/kg was administered IP after a 5 hr fast to 14 week old wildtype (filled circles; n=8) and *Imp2*$^{-/-}$ (open circles; n=8) mice maintained on HFD. The preinjection glucose values were slightly lower in the *Imp2*$^{-/-}$ ($p=0.08$), whereas values after insulin injection were all significantly lower ($p<0.02$ or lower).

D) Immunoblots of insulin receptor beta subunit, Akt, Akt(Ser473-P) in liver, skeletal muscle and WAT and S6K and S6K(389-P) in skeletal muscle and liver. Three pairs of

wildtype and *Imp2*$^{-/-}$ female mice 30 weeks age on a HFD were sacrificed 7 min. after IP injection of insulin (5U/kg) and extracts were subjected to immunoblot as indicated. E) The ratio of insulin receptor beta subunit, Akt, Akt(Ser473-P), S6K and S6K(389-P) in tissues of *Imp2*$^{-/-}$ mice relative to wildtype mice. The polypeptide immunoblots shown in 3D were quantified; the Akt-and S6K-phosphopeptide immunoblots were normalized for respective polypeptide content. The value for each in the *Imp2*$^{-/-}$ was divided by the corresponding value in the wildtype mice and the ratio is shown. *p<0.05, **p=<0.01 different from a ratio of 1.

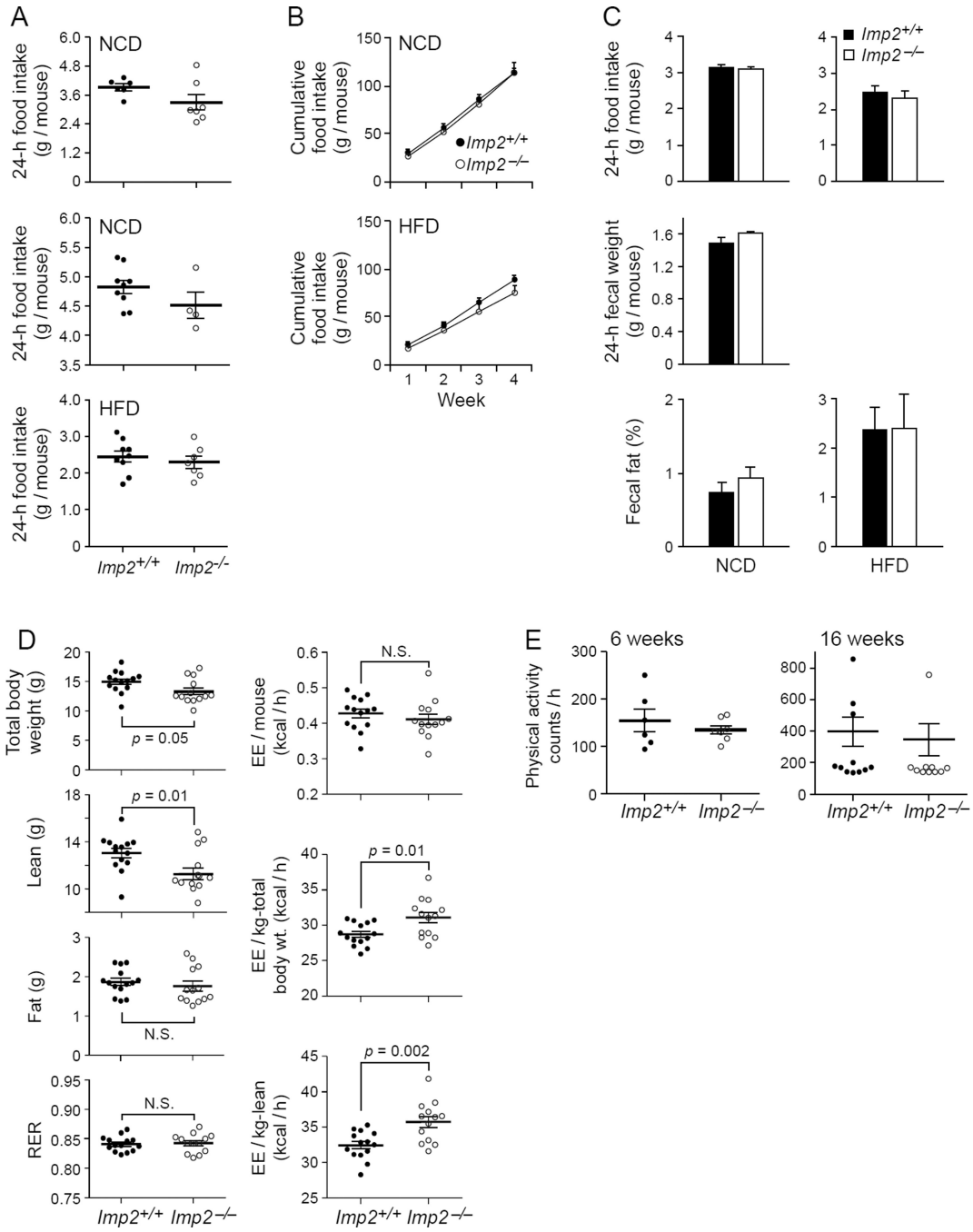

Figure 4. Food intake, fecal fat, energy expenditure in wildtype and *Imp2*$^{-/-}$ mice

A) Food intake over 24 hours at two ages. Upper: food intake of male wildtype (avg weight 19.1 g) and *Imp2*$^{-/-}$ (avg weight: 15.3g) mice at 4 weeks age. Middle: food intake of male wildtype and *Imp2*$^{-/-}$ mice at 16 weeks age on NCD (left; avg weight:wildtype-29.1g; *Imp2*$^{-/-}$ =27g); Lower: 16 week old male mice on HFD (right; avg weight: wildtype=37g; *Imp2*$^{-/-}$ =30.9g). See also Fig. S3A.

B) Cumulative food intake of wildtype (filled circles) and *Imp2*$^{-/-}$ (open circles) male mice measured weekly from 17–20 weeks age on NCD and HFD. Wildtype n=9, *Imp2*$^{-/-}$ n=7 for both diets.

C) Food intake, fecal weight and % fecal weight as TG on a NCD (left) and HFD (right); complete collection of feces on HFD not obtained. Three cages each containing three wildtype or *Imp2*$^{-/-}$ male mice, 18 to 19 weeks age were used for each diet.

D) Body weight, composition, respiratory quotient and energy expenditure of wildtype and *Imp2*$^{-/-}$ male mice at 4 weeks age after 4 days on a high fat diet. Fourteen wildtype and thirteen *Imp2*$^{-/-}$ male mice were placed in acclimatization cages for three days before initiating three days measurements of oxygen and carbon dioxide exchange. A HFD was started one day before calorimetry and continued; the data shown is from the last two days of claorimetry. Body weight and composition was measured at the finish of the calorimetry. Food intake is shown in 4A, upper. See also Fig. S3B.

E) Physical activity per 24 hrs in X-Y direction, Left: 14 pairs of 6 week old wildtype (avg.weight 19.1 g) and *Imp2*$^{-/-}$ (avg.weight: 15.3g) male mice on normal chow. Right: 12 pairs of wildtype (avg.weight: 29.1g) and *Imp2*$^{-/-}$$^{-/-}$(avg.weight: 27g) mice at 16 weeks on NCD.

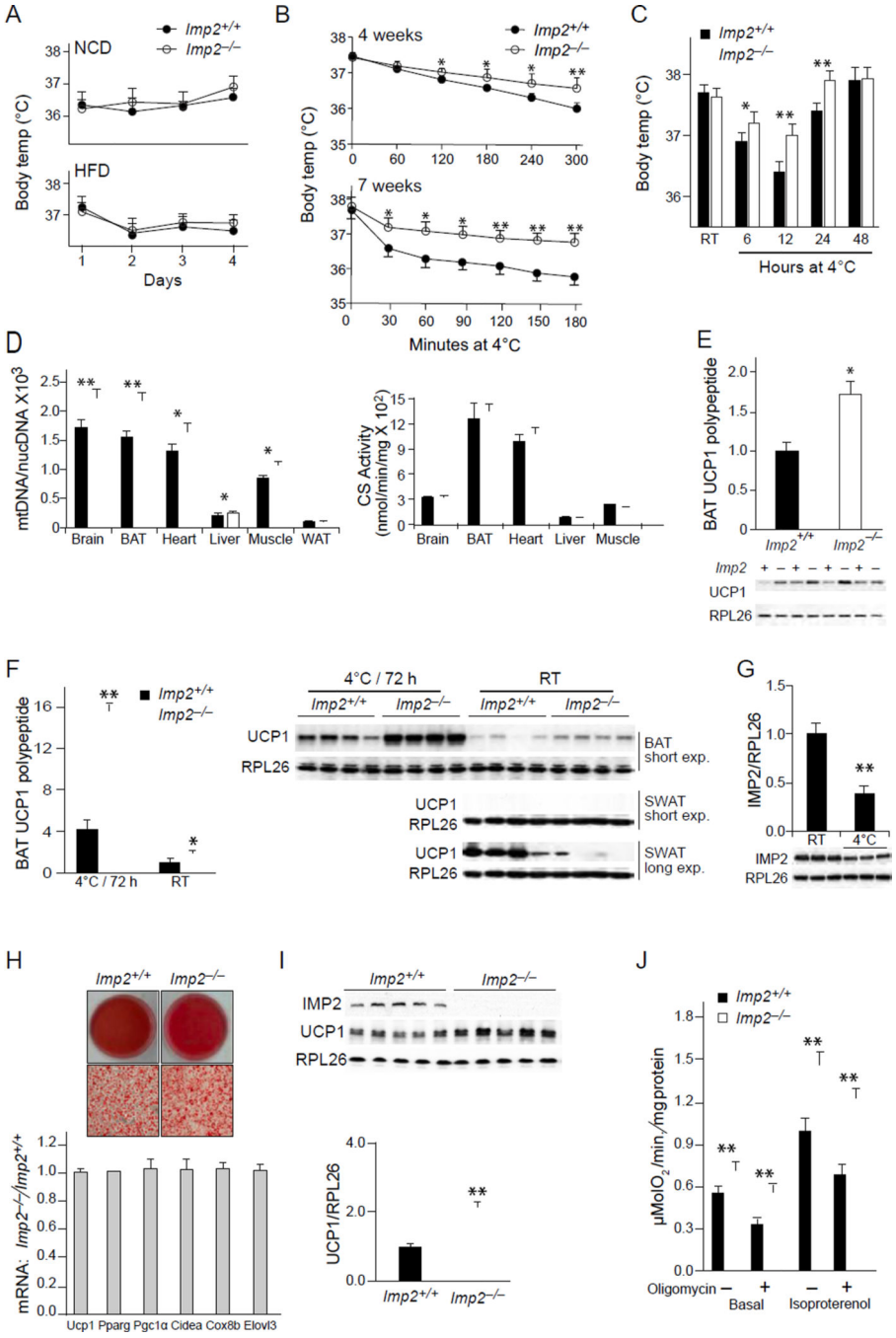

Figure 5. Body temperature regulation and mitochondrial abundance in wildtype and *Imp2*$^{-/-}$ mice and brown adipocyte UCP1 expression and oxygen consumption

A) Rectal body temperature measured 4 consecutive days in 20 week old male mice maintained on NCD (upper: WT n=11; avg weight: 34.7 gms, *Imp2*$^{-/-}$ n=9, avg weight=27.5g) or on a high fat diet (lower; WT n=9; avg weight: 48.1 gms; *Imp2*$^{-/-}$ n=7, avg weight=34.9g).

B) Body temperature in the first hours after exposure to 4°C. Rectal temperature was measured in 5 pairs of 28d old wildtype (avg. 14.7g) and *Imp2*$^{-/-}$ (avg. 13.1g) male mice

directly after weaning (upper) and in 12 pairs of 7 week old wildtype (avg. 20.7g) and *Imp2*$^{-/-}$ (avg. 17.6g) male mice maintained on NCD, followed by their transfer from room temperature to 4°C in individual precooled cages; rectal temperature was measured at 60min. (upper) or 30 min. (lower) intervals. *p<0.05; **p<0.01.

C) Body temperature during a 48 hour exposure to 4°C. Rectal temperature was measured in ten pairs of 7 week old wildtype (avg. 21.2g) and *Imp2*$^{-/-}$ (avg. 17.8g) male mice maintained on NCD, followed by their transfer from room temperature to 4°C as in B and rectal temperature was measured at the intervals shown. *p<0.05; **p<0.01.

D) Mitochondrial DNA and Citrate Synthase activities in selected tissues of wildtype and *Imp2*$^{-/-}$ mice. For measurement of Citrate Synthase (right), five pairs of 36 d wildtype and *Imp2*$^{-/-}$ female mice maintained on NCD were sacrificed and the tissues indicated were rapidly frozen; activities were determined spectrophotometrically (Frazier and Thorburn). Values for the respiratory chain enzyme activities Complexes I-IV in these same tissues are found in Sup. Fig. S4. The ratio of mitochondrial DNA to nuclear DNA (left) was determined in three independent experiments; DNA was extracted by phenol-chloroform from littermate pairs of wildtype and *Imp2*$^{-/-}$ mice placed on a HFD after weaning and sacrificed 3 days thereafter. The abundance of mitochondrial DNA and nuclear DNA was determined through QPCR for DNA encoding *ND1* and *Pecam1* respectively. The ratio of Ct values from three independent experiments, representing 10 pairs of wildtype and *Imp2*$^{-/-}$ mice is shown. *=p<0.05, **=p<0.01.

E) UCP1 polypeptide abundance in brown fat of young wildtype and *Imp2*$^{-/-}$ mice. The interscapular BAT depot was removed from 4 pairs of 39 d old wildtype (avg. 18.3 g) and *Imp2*$^{-/-}$ (avg. 16.1g) male mice maintained on HFD after weaning at 28d. Each depot was divided in two; an extract prepared from one half was immunoblotted for UCP1 and rpL26 as shown and RNAwas extracted from the other half, for measurement of *Ucp1* and *Gapdh* mRNA as shown in Sup. Figure S5B.

F) UCP1 polypeptide abundance in brown and white fat of older wildtype and *Imp2*$^{-/-}$ mice. The interscapular brown fat was excised from 16 week old wildtype and *Imp2*$^{-/-}$ male mice maintained on normal chow at room temperature and after three days at 4°C; the inguinal fat pads were excised from mice maintained at room temperature. A longer exposure is needed to detect UCP1 polypeptide in WAT than in BAT. The Ucp1 and Gapdh mRNAs in BAT from 16 week old mice maintained at RT or after 3 days at 4°C are shown in Sup. Fig. S5C.

G) Cold exposure reduces BAT IMP2 polypeptide. Five week old male *Imp2*$^{+/+}$ maintained on HFD from weaning were either left at room temperature or exposed to 4°C for 72h. The mice were sacrificed and an extract of interscapular BAT was immunoblotted for IMP2 and RPL26. **=p<0.01.

H) Stromal vascular cells from wildtype and *Imp2*$^{-/-}$ brown fat exhibit comparable differentiation into brown adipocytes in vitro. SVCs isolated from the interscapular brown fat of 33 day old *Imp2*$^{-/-}$ and *Imp2*$^{+/+}$ mice were differentiated in vitro into adipocytes; a representative oil-red-O stain of the cells post-differentiation is shown. RNA was extracted and analyzed by QPCR for the transcripts indicated; the abundance of each was normalized using the abundance of *Gapdh* mRNA and the ratio of *Imp2*$^{-/-}$ /*Imp2*$^{+/+}$ (+/− SED) for each mRNA is shown.

I) *Imp2*$^{-/-}$ brown adipocytes differentiated in vitro contain higher levels of UCP1 polypeptide than wildtype. Five sets of *Imp2*$^{-/-}$ (white bar) and *Imp2*$^{+/+}$ (black bar) stromal vascular cells, each set consisting of SVCs pooled from the interscapular BAT of four 33d old mice, were differentiated in vitro as in Fig. 5H. Extracts were immunoblotted for the polypeptides indicated; the ratio of UCP1/RPL26 polypeptides is shown. **=p<0.01.

J) *Imp2*$^{-/-}$ brown adipocytes differentiated in vitro exhibit higher total and uncoupled oxygen consumption than wildtype. The respiration of five sets of *Imp2*$^{-/-}$ (white bars) and *Imp2*$^{+/+}$ (black bars) brown adipocytes, differentiated in vitro and pretreated for 6h with or without isoproterenol (10μM), was measured as single cell suspensions in the presence or absence of oligomycin (1μM) using a Clark electrode. **=p<0.01.

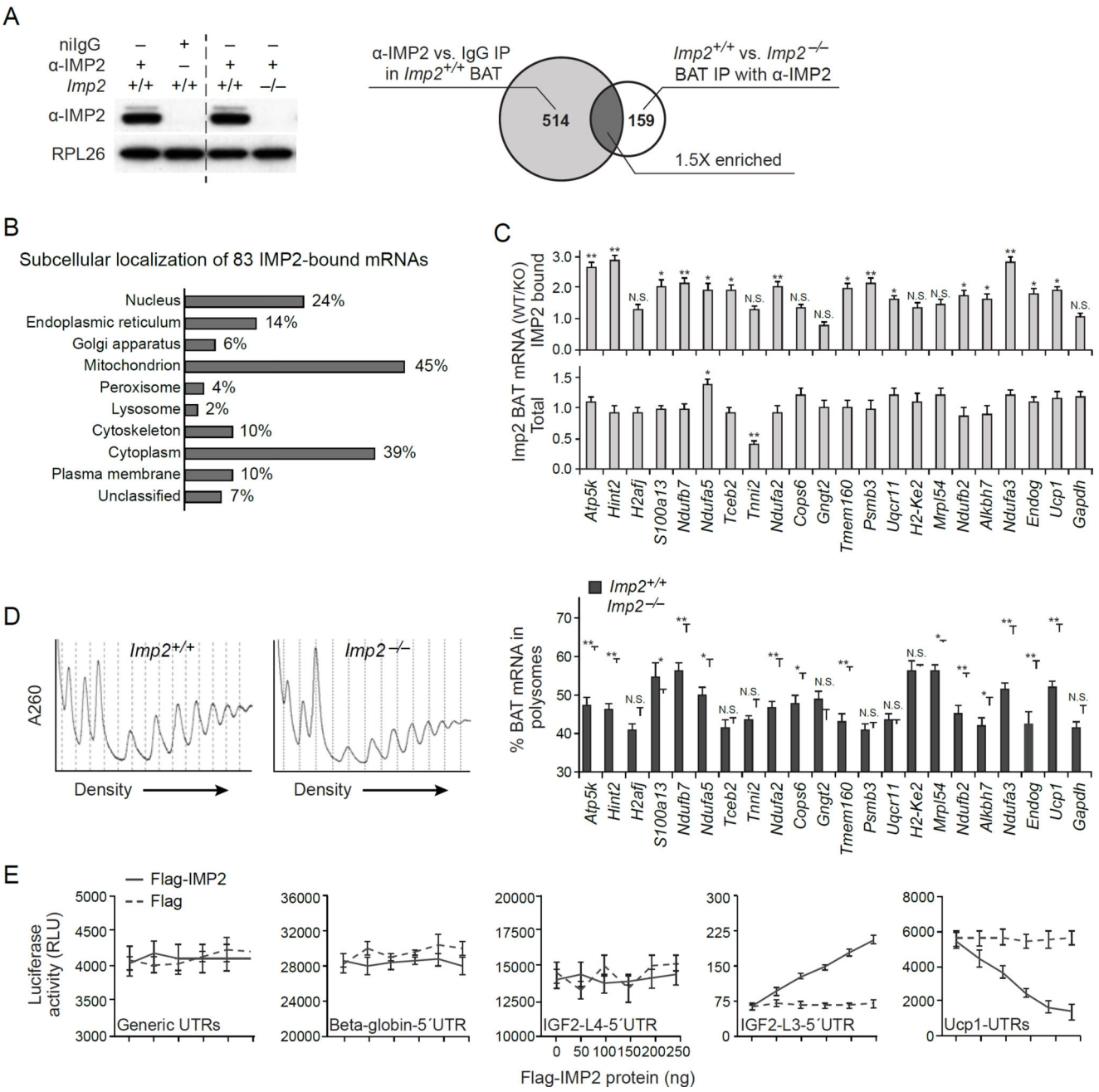

Figure 6. IMP2 binds *Ucp1* mRNA and negatively regulates its translation in vivo and in vitro

A) Identification of abundant mRNAs bound to IMP2 in brown fat by RNA seq. Anti-IMP2 IPs were prepared from wildtype and *Imp2*$^{-/-}$ BAT; separately, anti-IMP2 and nonimmune IgG IPs were prepared from wildtype BAT. The RNA bound to the various IPs was purified and equal amounts were subjected to RNA sequencing as described in methods, in parallel with aliquots of polyA+RNA from wildtype and *Imp2*$^{-/-}$ BAT. RNA abundance in the IPs was adjusted for the abundance of that RNA in the corresponding total RNA and RNAs enriched in the IMP2 IP were identified; considering only RNAs yielding ≥ 100 reads in the

IMP2 IPs from wildtype BAT, 83 mRNAs were found to be enriched 1.5-fold or greater in the IMP2 IPs by comparison to both the IgG IP or the IMP2 IP from *Imp2*$^{-/-}$ BAT.
B) Subcellular localization of IMP2-bound RNAs in BAT.
C) QPCR confirmation of relative enrichment of candidate IMP2 bound BAT RNAs as identified by RNA seq. RNA was extracted from a set of IMP2 IPs prepared from wildtype and *Imp2*$^{-/-}$ BAT, distinct from those used in 7A, and 21 of the 83 candidate IMP2 bound BAT RNAs identified in 6A were analyzed by QPCR. The upper bar graph shows a ratio of RNA abundance in the IP from wildtype BAT divided by it abundance in the IMP2 IP from *Imp2*$^{-/-}$ BAT. The lower bar graph shows the ratio of the abundance of the same RNAs in the total RNA extracted from wildtype and *Imp2*$^{-/-}$ BAT. *Gapdh* RNA is included as a control previously shown to not bind IMP2. * = $p<0.05$, ** = $p<0.01$.
D) The polysomal abundance of candidate IMP2-associated RNAs in wildtype and *Imp2*$^{-/-}$ BAT. Aliquots of postnuclear extracts of BAT from four wildtype and four *Imp2*$^{-/-}$ mice, placed at 4C for 24 h prior to sacrifice, were analyzed for *Ucp1* mRNA and protein as shown in Fig. S5 and then pooled. Aliquots containing equal amounts of lysate were subjected to sucrose density gradient centrifugation; the RNA in the total extract loaded on the gradient and the RNA in the pooled polysomal fractions were extracted, the abundance of each RNA indicated was measured by QPCR and the percent of polysomal localization was calculated as the ratio of polysomal abundance divided by the abundance in the total loaded, X100. Filled bars=wildtype and open bars= *Imp2*$^{-/-}$ BAT; * = $p<0.05$, ** = $p<0.01$.
E) The effect of IMP2 on the translation of Luciferase RNA flanked by heterologous untranslated segments. The coding sequence of firefly Luciferase RNA was fused to (from the left) a generic 5' and 3'UTR; the human beta globin 5'UTR and a generic 3'UTR; the human *IGF2* leader 4 5'UTR and a generic 3'UTR; the human *IGF2* leader 3 5'UTR and a generic 3'UTR and the murine *UCP1* 5'UTR and 3'UTR. These RNAs were transcribed in vitro and used to program a reticulocyte lysate. Extracts of 293 cells transfected with either an empty flag vector (mock, dashed) or the same vector encoding flag-IMP2 (solid) were adsorbed to immobilized anti-flag MC antibody, and eluted with flag peptide. The content of flag-IMP2 was estimated by C.B. stain, and aliquots of the flag-IMP2 (solid) and corresponding amounts of the mock flag eluate (dashed) were added to the lysates. Translation was estimated by the gain in luciferase activity after incubation for 30 minutes at 30C°.